

1 **Origin and Evolution of a CO₂-Rich Gas Reservoir Offshore Angola:**
2 **Insights from the Gas Composition and Isotope Analysis**

3 **Junjie Liu^{1,2,3,4}, Magali Pujol⁵, Honggang Zhou⁵, David Selby⁴, Jie Li^{2,3}, and Bin**
4 **Cheng^{3,6}**

5 ¹Guangdong Key Lab of Geodynamics and Geohazards, School of Earth Sciences and
6 Engineering, Sun Yat-sen University, Guangzhou 510275, China

7 ²State Key Laboratory of Isotope Geochemistry, Guangzhou Institute of Geochemistry,
8 Chinese Academy of Sciences, Guangzhou 510640, China.

9 ³CAS Center for Excellence in Deep Earth Science, Guangzhou, 510640, China.

10 ⁴Department of Earth Sciences, Durham University, Durham, DH1 3LE, UK.

11 ⁵TOTAL, Centre Scientifique et Techniques Jean-Féger, Avenue Larribau, 64018 Pau,
12 France.

13 ⁶State Key Laboratory of Organic Geochemistry, Guangzhou Institute of Geochemistry,
14 Chinese Academy of Sciences, Guangzhou 510640, China.

15

16 Corresponding author: Junjie Liu (864824239@qq.com/liu.junjie@gig.ac.cn)

17 Magali Pujol: magali.pujol@total.com

18 Honggang Zhou: honggang.zhou@total.com

19 Jie Li: jieli@gig.ac.cn

20 Bin Cheng: chengbin@gig.ac.cn

21

22 **Highlights**

- 23 • A pre-salt reservoir in the Kwanza Basin is rich in bitumen, CO₂ and methane;
- 24 • This reservoir is SHGS with mantle-derived CO₂ and late mature thermogenic
- 25 CH₄;
- 26 • The $\delta^{13}\text{C}$ indicates mixed sapropelic, humic and abiotic origins for
- 27 hydrocarbons;
- 28 • Rapid oil generation occurred due to high thermal gradient or fast deposition;
- 29 • Similarity to Brazilian basins may indicate great petroleum potential for Angola.

30 **Abstract**

31 The pre-salt sections of the offshore Kwanza Basin, Angola are potentially petroliferous
32 reservoirs like their Brazilian counterparts on the other side of the South Atlantic Ocean.
33 In this study, a pre-salt reservoir of the offshore Kwanza Basin was found to contain
34 solid bitumen and gas of high portions of CO₂ (ca. 83%) and methane (ca. 16%). The
35 chemical and isotopic (C, H and He) compositions of the gas indicate that the CO₂ is
36 primarily mantle-derived while the gaseous hydrocarbons are mainly late mature
37 thermogenic gas. The Barremian-Aptian Red Cuvo Formation with sapropelic and
38 humic organic matter and an average TOC content of 1.7% could be the principal source
39 of the bitumen and gaseous hydrocarbons in the reservoir. Rapid oil generation since
40 the source rock sedimentation could have occurred as a result of the fast and thick salt
41 deposition or the high thermal gradient created by the crustal thinning and magmatism
42 during the South Atlantic Ocean opening. The $\delta^{13}\text{C}$ of gaseous hydrocarbons also
43 indicates their mixed origins of sapropelic and humic organic matters and possible
44 abiotic processes.

45 This reservoir is similar in the origin of CO₂ and geological background to some pre-
46 salt reservoirs in the Brazilian basins. Such similarities with prolific petroleum systems
47 may imply great petroleum potential in the pre-salt sections of the offshore Kwanza
48 Basin, Angola.

49 **Keywords:** Kwanza Basin, Angola; Pre-salt reservoir; CO₂; petroleum potential; South
50 Atlantic Ocean opening.

51 **1. Introduction**

52 The separation of Southern Africa and South America during the opening of the South
53 Atlantic Ocean in the Early Cretaceous resulted in the development of conjugated
54 passive continental marginal basins that share a common tectonic evolution and
55 sedimentary history (Figure 1; Blaich et al., 2011; Kukla et al., 2018; Quirk et al., 2013).
56 Confined between the volcanic lineaments of the Walvis Ridge and the Rio Grande
57 Rise to the south and the Ascension Fracture Zone to the north, the central segment of
58 the South Atlantic Ocean is characterized by pervasive Aptian salt deposition and
59 considerable petroleum reserves discovered in the pre-salt carbonate reservoirs in the
60 offshore Brazilian Santos and Campos basins (Aslanian et al., 2009; Ceraldi and Green,
61 2017; Karner and Gambôa, 2007; Kukla et al., 2018; Quirk et al., 2013). This has led
62 to the increase of petroleum exploration activities in the pre-salt plays on the Western
63 African side of the South Atlantic Ocean with discoveries, e.g., in the Orca, Cameia,
64 and Azul areas of the offshore Kwanza Basin, Angola (Figure 1; Despinois et al., 2014;
65 Greenhalgh et al., 2012; Koning, 2014).

66 A recent study discovered a pre-salt reservoir of the offshore Kwanza Basin, Angola
67 containing bitumen and gas (Liu et al., 2022) and proposed a bitumen formation model.
68 Here, we present the study on the gas of this reservoir through chemical and isotopic
69 composition analysis to understand its fluid origin and evolution history as an example
70 to understand the petroleum potential of the Angolan pre-salt reservoirs.

71 **2. Geological background**

72 The Early Cretaceous deposition of the central segment of the South Atlantic Ocean
73 can be defined as pre-rift, rift, sag, salt basin and post-salt stages in the context of the

74 South Atlantic Ocean opening (Ceraldi and Green, 2017). Before the invasion of
75 seawater and formation of the salt basin, the Walvis Ridge and the Rio Grande Rise
76 volcanic lineaments formed by mantle plume activities blocked the seawater to the
77 south and thus the rift basins of the central segment of the South Atlantic Ocean were
78 fluvial-deltaic and lacustrine basins (Thompson et al., 2015). As a result, the pre-salt
79 sedimentary stratigraphy can be divided into three phases (Ceraldi and Green, 2017).
80 The first phase was composed of the fluvial-lacustrine deposition from freshwater deep
81 basins created by the syn-rift grabens during the onset of continental break-up. The
82 second phase (Sag 1) was composed of mainly carbonate deposition from the possibly
83 interconnected fresh to brackish lakes during the widespread subsidence created by the
84 syn-kinematic stretching of the continental crust and/or continuous rifting. Lastly, the
85 third phase (Sag 2) was composed of microbial deposition from the under-filled,
86 alkaline and hyperalkaline lake formed as a result of the continuous subsidence (Ceraldi
87 and Green, 2017). Organic-rich mudstones were deposited in the deep lacustrine
88 environment which was limited in the grabens during the syn-rift phase but more
89 widespread during the Sag phase, e.g., the Bucomazi Formation and its equivalents in
90 the Lower Congo and Kwanza basins and the Lagoa Feia and Guaratiba formations of
91 the Brazilian Campos and Santos basins (Brownfield and Charpentier, 2006; Burwood,
92 1999; Saller et al., 2016).

93 The subsidence of the volcanic barriers due to the northward-propagating rifting of the
94 supercontinent Gondwana during the Late Aptian induced periodic or episodic seawater
95 invasion and the deposition of thick and extensive salt deposits in the central segment
96 of the South Atlantic Ocean (Ceraldi and Green, 2017; Karner and Gambôa, 2007;
97 Quirk et al., 2013; Torsvik et al., 2009). Sea-level rose progressively following the salt

98 deposition, leaving deposits of restricted marine carbonate and evaporite before the
99 open marine sedimentation took over from the Late Cretaceous (Saller et al., 2016;
100 Torsvik et al., 2009).

101 In the southern offshore Kwanza Basin (or named the Benguela Basin), a well has been
102 drilled through the studied reservoir which penetrates through the salt of the Aptian
103 Loeme Formation (2616.5 m; 2687.5–5304 m), the pre-salt Chela Formation (216 m;
104 5304–5520 m) with carbonate and silicified carbonate deposits, the Grey Cuvo
105 Formation (133 m; 5520–5653 m) with fine grain siliciclastic sandstone and clay
106 deposits and the Barremian-Aptian lacustrine Red Cuvo Formation (397 m; 5653–6050
107 m) with mixed deposits of siltstone, black shale, thin carbonate interlayer, and igneous
108 units (Figure 1).

109 **3. Samples and methods**

110 Sidewall core samples were collected from the pre-salt Chela, Grey Cuvo and Red Cuvo
111 formations (Table 1) for the total organic carbon (TOC) content measurements, maceral
112 identification and Rock-Eval analysis. All the analyses were run in CSTJF-TOTAL
113 Facilities in Pau, France. The TOC contents of the powdered samples were determined
114 with a LECO CS-400 carbon/sulfur analyzer after the treatment with hydrochloric acid.
115 The preparation of samples for optical analysis, identification of organic matter type,
116 and measurement of vitrinite reflectance followed standard methods, i.e., ASTM
117 D2797/D2797M-11a (2011a), ASTM D2799-12 (2012), and ASTM D7708-11
118 (2011b). The maceral examination was performed using a LEICA DM6000M
119 microscope. Reflectance measurements were carried out on vitrinite and bitumen under

120 reflected white incident light in oil immersion. Rock-Eval analysis was conducted with
121 Rock-Eval 6 (Table 2).

122 Four down-hole pressurized fluid samples were taken from the Chela and Red Cuvo
123 formations with the Multi-sample Production Sample Receptacle (MPSR) of the
124 Schlumberger MDT Modular Formation Dynamics Tester and measured at CSTJF-
125 TOTAL Facilities (Table 3). The gas composition was measured with an Agilent 8890
126 GC chromatography equipped with an Agilent HP-PLOT Al₂O₃ S column (25 m × 0.32
127 mm × 8 μm) and flame ionization and thermal conductivity detectors. The carbon
128 isotope compositions of the hydrocarbons and CO₂ were analyzed by Gas
129 Chromatography-Combustion Isotope-Ratio Mass Spectrometry (GC-C-IRMS) with an
130 Agilent 6890N equipped with an Agilent PoraPLOT Q column (25 m × 0.32 mm × 10
131 μm) and IsoPrime 100. The hydrogen isotope compositions of the hydrocarbons were
132 measured by Gas Chromatography-Thermal Conversion-Isotope Ratio Mass
133 Spectrometry (GC-TC-IRMS) with a ThermoFisher Trace1310 equipped with a
134 PoraPLOT Q column (25 m × 0.32 mm × 10 μm) and Delta V Advantage. The
135 temperature programs for the C and H isotope composition analyses were starting from
136 50 °C and kept for 3 mins and then increasing the temperature to 190 °C at 30 °C/min.
137 The carrier gas was Helium. The helium concentration and isotope composition of the
138 samples were analyzed following Györe (2015) with a Mass Analyzer Product (MAP)
139 215-50 mass spectrometer.

140 **4. Results**

141 The organic matter in the Chela Formation carbonate rock reservoir is characterized as
142 abundant pore-filling anisotropic bitumen with no autochthonous organic matter

143 (Figure 2a-b). The TOC (purely bitumen) contents are 0.4–4.5% with an average of
144 1.7% (Table 1). The bitumen has no fluorescence and is characterized by relatively high
145 bitumen reflectance (BR_o) of 1.88–1.98% (equivalent VR_o of 1.56–1.62%; Table 1;
146 Jacob, 1989). The Grey Cuvo Formation samples are carbonate- and argillaceous-rich
147 siltstones with small-size humic coaly fragments, e.g., inertinite and vitrinite (Figure
148 2c-e). The TOC contents are in the range of 0.6–1% with an average of 0.74% (Table
149 1). The organic matter exhibits zero fluorescence and the vitrinite reflectance is between
150 1.45 and 1.52 % (Table 1). The Red Cuvo Formation consists of siliciclastic rocks
151 bearing various contents of carbonate and pyrite. The organic matter is a mix of
152 sapropelic micro-granular organic matter and terrestrial land plant debris (humic coaly
153 fragment; Figure 2f-h). Scarce anisotropic bitumen is also observed (Figure 2h). The
154 TOC contents are 1.1–3.9% with an average of 1.7% (Table 1). Vitrinite reflectance
155 values in the Red Cuvo Formation show a general increase with depth from ca. 1.7% at
156 5791.5 m to 2.1% at 6015.0 m (Table 1). The low Rock-Eval parameters of the Red
157 Cuvo Formation samples indicate that their hydrocarbon generation potential has been
158 exhausted (Table 2).

159 The four fluids sampled from the Chela and Red Cuvo formations are predominantly
160 comprised of CO_2 (ca. 82–84%) and CH_4 (ca. 14–17%; Table 3). The CH_4 accounts for
161 ca. 93–96% of the total hydrocarbons. The hydrocarbon composition, $\delta^{13}C$ and δ^2H are
162 homogeneous for the shallower three samples while being slightly different from the
163 deepest 5980.8 m sample in general (Table 3; Figure 3-4). Helium concentrations vary
164 between 1 and $1.4 \times 10^{-4} \text{ cm}^3/\text{cm}^3$ (1 atm and 15 °C; Table 3). The molar ratio $^3He/^4He$
165 is presented as R/R_a , which represents the $^3He/^4He$ value of the sample (R) divided by

166 that of air (R_a , 1.384×10^{-6} ; Clarke et al., 1976). The R/R_a values are 4.4–4.7 while the
167 $\text{CO}_2/{}^3\text{He}$ ratios are ca. 0.89 to 1.32×10^9 .

168 **5. Discussion**

169 **5.1 CO₂ source(s)**

170 The sources for CO_2 in geological reservoirs can be magmatism, regional and contact
171 metamorphism, marine carbonates, biotic decay, and the breakdown of coaly Type III
172 organic matters (Procesi et al., 2019; Wycherley et al., 1999). The natural gases in this
173 study are composed of ca. 82–84 mol% of CO_2 . For most reservoirs with abundant CO_2 ,
174 e.g., > 70 mol%, the major sources of the CO_2 are typically magmatism and
175 metamorphism (Györe, 2015; Wycherley et al., 1999). The fact that the $\delta^{13}\text{C}$ values of
176 the CO_2 of the samples in this study are ca. -3.9‰ (Table 3) also indicates that their
177 dominant CO_2 sources could include magmatism ($\delta^{13}\text{C}_{\text{CO}_2}$ of ca. -7 to -4‰) and regional
178 metamorphism ($\delta^{13}\text{C}_{\text{CO}_2}$ of ca. -10‰ to 0; Györe, 2015; Jenden et al., 1993b; Wycherley
179 et al., 1999).

180 A clear mantle signature is identified for the studied gas samples through their excessive
181 primordial ${}^3\text{He}$ compared to air, as the R/R_a values are as high as ca. 4.5 (Table 3) which
182 is often the characteristic of mantle-originated fluids (Porcelli et al., 2002). Meanwhile,
183 the samples possess an evident excess of radiogenic ${}^4\text{He}$ compared with typical MORB
184 (Mid-Ocean Ridge Basalt) noble gas, as their R/R_a value of ca. 4.5 is lower than the
185 typical value of 8 for MORB-type noble gas (Graham, 2002). Such radiogenic ${}^4\text{He}$
186 could be produced by the alpha decay of U and Th, elements that are rare in the reservoir
187 lithologically dominated by carbonates but can be abundant in the clastic sedimentary

188 rocks and/or igneous rock. The $\text{CO}_2/{}^3\text{He}$ ratios of the studied gases are $0.89\text{--}1.32 \times 10^9$
189 (Table 3) which are consistent with the typical range of $\text{CO}_2/{}^3\text{He}$ ratios for pure
190 magmatic-sourced fluids, i.e., around 10^9 to 10^{10} (Ballentine et al., 2002). The value
191 below this range, i.e., 0.89×10^9 for the deepest sample, indicates that the gas may have
192 been subjected to CO_2 loss by dissolving into the aquifer. Thus, the CO_2 in the studied
193 reservoir is mainly mantle-derived although there may have been minor contributions
194 from metamorphism and organic matter (Figure 3e-f).

195 The South Atlantic Ocean opening was associated with active magma activities (Masse
196 and Laurent, 2016). Three main episodes of magma activities are recognized in the
197 South Kwanza Basin and they could have been significant source(s) of CO_2 (Comin-
198 Chiamonti et al., 2011; Denis and Kluska, 2017; Jerram et al., 2019; Kukla et al.,
199 2018; Marzoli et al., 1999; Masse and Laurent, 2016). The earliest major magmatic
200 episode is the Paraná-Etendeka flood basalt province (ca. 132 Ma; Marzoli et al., 1999)
201 which is characterized by tholeiitic lava flows, dykes and volcanoclastic sediments
202 underlying the Early Cretaceous sedimentary succession. It only lasted for a short
203 duration of 3–4 m.y. (Jerram et al., 2019; Marzoli et al., 1999) and took place much
204 earlier than the deposition of caprock of the reservoir in this study, i.e., the Loeme
205 Formation salt (ca. 117–113 Ma; Quirk et al., 2013). Thus, it is unlikely to be the main
206 source of CO_2 in the studied reservoir.

207 The second is an Aptian episode of tholeiitic magmatism during the syn- to early post-
208 rift phase of the South Atlantic Ridge breakup which intruded the Barremian to Aptian
209 sedimentary units including the salt (Denis and Kluska, 2017; Jerram et al., 2019; Marsh
210 and Swart, 2018; Marzoli et al., 1999; Quirk et al., 2013). This magmatic episode is
211 well-developed offshore. The latest one is an Albian-Turonian alkaline magmatic

212 episode (Jerram et al., 2019; Marzoli et al., 1999; Quirk et al., 2013) which has been
213 interpreted to originate from a mantle perturbation at the base of the lithosphere like the
214 Cameroon Volcanic Line (Reusch et al., 2010). The origin of CO₂ cannot be
215 unambiguously constrained to either of these two later magmatic episodes through the
216 $\delta^{13}\text{C}$ of CO₂ and He signatures.

217 In a recent study, CO₂ was believed to have induced the bitumen formation through
218 asphaltene precipitation and thermal cracking in this reservoir (Liu et al., 2022). The
219 timing of this CO₂-induced bitumen formation process was constrained by the Re-Os
220 radioisotope geochronometer to be 116 ± 29 Ma (2σ ; Liu et al., 2022). Thus, the CO₂
221 responsible for the bitumen formation should be originated from the second episode
222 (Aptian) magma activity. The third Albian magmatic episode may have also contributed
223 CO₂ to the studied reservoir, although the amount is difficult to estimate. It is worth
224 noting that there is still a considerable quantity of gaseous hydrocarbons left in the
225 reservoir currently as will be discussed in the following sections. The gaseous
226 hydrocarbons are mainly thermogenic and should be generated through the source rock
227 maturation and possibly the oil thermal cracking during the Aptian CO₂ alteration. If
228 there has been Albian CO₂ charged into the studied reservoir, it was incapable of clearly
229 expelling these antecedent hydrocarbons, and the earlier CO₂ as well. Besides mantle
230 CO₂, these two magma episodes could also produce CO₂ through contact
231 metamorphism of carbonates (Wycherley et al., 1999).

232 **5.2 Gaseous hydrocarbon source(s)**

233 Natural gas may have either biotic or abiotic origins. Biotic gas is generated from
234 organic matter through thermogenic and microbial processes. Abiotic gases can form

235 from magmatism and gas-water-rock reactions, e.g., Fischer-Tropsch Type (FTT)
236 synthesis (Etiope and Oze, 2022; Etiope and Sherwood Lollar, 2013; Etiope and
237 Whiticar, 2019). The gas composition and stable C and H isotope composition are
238 often used to identify the origins of the gas. The $\delta^{13}\text{C}$ trend of the gaseous hydrocarbons
239 of the fluids in this study are $\delta^{13}\text{C}_1 \approx \delta^{13}\text{C}_2 < \delta^{13}\text{C}_3 < \delta^{13}\text{C}_4$ (Table 3; Figure 4), indicating
240 their predominantly biotic origin rather than a reversed $\delta^{13}\text{C}$ trend of $\delta^{13}\text{C}_1 > \delta^{13}\text{C}_2 >$
241 $\delta^{13}\text{C}_3 > \delta^{13}\text{C}_4$ for common abiotic gaseous hydrocarbons (Chung et al., 1988; Dai et al.,
242 2008; Jenden et al., 1993b).

243 It is indicated on the genetic diagrams of $\delta^2\text{H}-\text{CH}_4$, $\text{C}_1/(\text{C}_2 + \text{C}_3)$ and $\delta^{13}\text{C}-\text{CO}_2$ versus
244 $\delta^{13}\text{C}-\text{CH}_4$ that the gaseous hydrocarbons in the studied reservoir are dominant of late
245 mature thermogenic gas (Figure 3; Milkov and Etiope, 2018). Although close to the
246 secondary microbial zone (Figure 3a, c and e) and the arrow indicating oxidation
247 process (Figure 3d), the studied samples are unlikely to have such origin or to be
248 affected by such processes considering their burial depth of ca. 5000–6000 m. Although
249 it is indicated that the gas samples may have been altered by thermochemical sulfate
250 reduction (TSR) processes (Figure 3b and d), it is not supported by the absence of H_2S
251 (Table 3). The $\delta^{13}\text{C}-\text{CO}_2$ versus $\delta^{13}\text{C}-\text{CH}_4$ diagrams (Figure 3e-f) indicate that the CO_2
252 is compatible with the C stable isotope range of late mature thermogenic gas. There
253 may have also been some thermogenic CO_2 , although we have concluded that the CO_2
254 is mainly mantle-derived.

255 The organic-rich intervals of the pre-salt section in the Kwanza Basin are the mudstone,
256 marl and shales deposited in the deep lacustrine environment during both the Barremian
257 to Aptian syn-rift and sag stages (Brownfield and Charpentier, 2006; Burwood, 1999;
258 Ceraldi and Green, 2017; Danforth, 1998; Saller et al., 2016). The organic-rich strata

259 drilled through by the studied well are the Barremian-Aptian Red and Grey Cuvo
260 formations. The vitrinite R_o values of these two formations are 1.7–2.1% and ca. 1.5%,
261 respectively, indicating that they have been mature and are in the stages of wet to dry
262 gas and condensate generation, respectively. Considering their thickness (397 m vs 133
263 m), average TOC contents (1.7% vs 0.74%) and generation potential (sapropelic
264 organic matter vs humic coaly fragments), the Red Cuvo Formation is more likely to
265 be the major source for the hydrocarbons in the studied reservoir than the Grey Cuvo
266 Formation. Besides, the presence of the pore-filling bitumen in the Chela Formation
267 carbonate reservoir indicates that there was charge(s) of crude oil for which the
268 sapropelic organic matter of the Red Cuvo Formation should be the principal source.
269 Moreover, the humic contribution to the gas could be attributed to the coaly fragments
270 and terrestrial land plants of the Grey and Red Cuvo formations. Partial thermal
271 cracking of crude oil during the bitumen formation process could also generate light
272 hydrocarbons (Liu et al., 2022).

273 The samples are also very close to and even within the abiotic zone on the genetic
274 diagrams indicating possible abiotic contribution to the gaseous hydrocarbons in the
275 studied reservoir (Figure 3). Gases from pure and active magmatic systems generally
276 contain 10^{-4} to 0.5% CH_4 (Procesi et al., 2019) which could account for 0.05–2.56% of
277 the current methane in the studied reservoir if the loss and the contributions other than
278 magmatism of CO_2 are neglected. Besides, the geometric mean molar ratio of $CH_4/{}^3He$
279 is 3×10^6 for the uncontaminated mantle-derived fluids from spreading ridges (Jenden
280 et al., 1993b). The $CH_4/{}^3He$ values of the fluids from the reservoir in this study are in
281 the range of $1.7\text{--}2.6 \times 10^8$ (Table 3). Thus, the methane derived from magmatism along
282 with the noble gases and CO_2 may account for ca. 1.2–1.8% of the total methane of the

283 reservoir in this study, although the result can be very different from this estimation
284 considering mantle heterogeneity. Both calculations from CO₂ and ³He indicate a low
285 contribution of CH₄ (maximum of 2.56%) from mantle or magmatism to the methane
286 budget of the studied reservoir. Besides, there hasn't been any hydrocarbon larger than
287 C₂H₆ found in mantle-derived gases so far (Liu et al., 2019).

288 Among the gas-water-rock reactions, Fischer-Tropsch Type (FTT) synthesis (Sabatier
289 reaction in the free gas phase) within ultramafic rocks is likely the only one that can
290 generate a considerable amount of methane (Etiope and Oze, 2022; Etiope and
291 Sherwood Lollar, 2013; Etiope and Whiticar, 2019). Abiotic methane can be generated
292 through FTT synthesis within the ultramafic rocks associated with magma activities,
293 e.g., the Albian-Turonian alkaline magmatic episode (Jerram et al., 2019; Marzoli et
294 al., 1999; Quirk et al., 2013). There are limitations on the FTT synthesis methane
295 production, e.g., catalysts; however, it can be a long-term active generating source for
296 methane and its production can potentially be comparable to thermogenic methane over
297 geological time (Etiope and Whiticar, 2019). Unfortunately, it is hard to quantify the
298 FTT synthesis contribution of methane in this reservoir.

299 Thus, the gaseous hydrocarbons in the reservoir of this study are mainly late mature
300 thermogenic gas with possible abiotic methane contributions from magmatism and FTT
301 synthesis according to the chemical and isotopic gas compositions of the gas.

302 **5.3 Further implications from the $\delta^{13}\text{C}$ of hydrocarbons**

303 The kinetic nature of the thermogenic natural gas generation process leads to the
304 expectation for the hydrocarbons with higher carbon numbers and the hydrocarbons

305 generated under higher maturity to have more positive $\delta^{13}\text{C}$ values (Tang et al., 2000;
306 Xia et al., 2013). Chung et al. (1988) reported the $\delta^{13}\text{C}$ of hydrocarbons on a plot as the
307 function of inverse carbon number, i.e., $\delta^{13}\text{C}_n$ vs $1/n$ (e.g., Figure 4). Based on an ideal
308 equation, the hydrocarbons should be on a straight line in such a diagram if they are
309 generated in a single pulse from the organic matter of the source rocks with
310 homogeneous $\delta^{13}\text{C}$ (Chung et al., 1988). However, deviation from the straight line and
311 even the $\delta^{13}\text{C}$ reversal to carbon number and maturity are often observed (Burruss and
312 Laughrey, 2010; Dai et al., 2004; Jenden et al., 1993a; Tilley et al., 2011; Xia et al.,
313 1999; Zumberge et al., 2012). Mixing of gases from different sources and/or generation
314 pulses, secondary cracking of crude oil and wet gas, diffusion and methane cracking
315 are proposed to be the causes of the $\delta^{13}\text{C}$ deviation and reversal of biotic hydrocarbons
316 (Burruss and Laughrey, 2010; Cheng et al., 2020; Dai et al., 2016; Jenden et al., 1993a;
317 Tilley et al., 2011; Tilley and Muehlenbachs, 2013; Xia et al., 2013; Zumberge et al.,
318 2012).

319 For the gas samples from the studied reservoir, the actual $\delta^{13}\text{C}_1$ of the shallower three
320 samples and the actual $\delta^{13}\text{C}_1$ and $\delta^{13}\text{C}_2$ of the deepest sample are heavier than the
321 projections, making the curves to be concave (Figure 4). The $\delta^{13}\text{C}_1$ and $\delta^{13}\text{C}_2$ are nearly
322 identical for the shallower three samples. The $\delta^{13}\text{C}_1$ is slightly heavier than the $\delta^{13}\text{C}_2$
323 for the 5980.8 m sample, i.e., the $\delta^{13}\text{C}$ is slightly reversed (Table 3).

324 The mixing of gases generated from either different sources or maturities is often
325 considered the cause of the isotope reversal first (Liu et al., 2019). Gases of humic
326 origin are often heavier in $\delta^{13}\text{C}$ than those of sapropelic origin in the same maturation
327 stages while abiotic methane is often heavier in $\delta^{13}\text{C}$ than biotic methane (Hunt, 1996).

328 The gaseous hydrocarbons in the studied reservoir are mainly of sapropelic origin, the
329 deviation of $\delta^{13}\text{C}_1$ and $\delta^{13}\text{C}_2$ to be heavier than the projections from the propane and
330 butanes in Chung's plot (Figure 4) can be attributed to the humic and abiotic (e.g.,
331 magmatic and FTT synthesis) contributions of methane and ethane. The humic
332 contribution should take the major responsibility for shifting the $\delta^{13}\text{C}$ positively
333 considering the appreciable amount of humic organic matter in both the over 100 m
334 thick Grey Cuvo Formation with average TOC content of 0.74% and the ca. 400 m thick
335 Red Cuvo Formation. Mantle-derived methane is generally characterized by $\delta^{13}\text{C}$ and
336 $\delta^2\text{H}$ heavier than -20‰ and -200‰, respectively (Etiope and Sherwood Lollar, 2013).
337 Although they are distinctly different from the corresponding values of ca. -32‰ and -
338 131 to -140‰ of the studied gas, the change it can make is limited due to its trace
339 contribution to the total methane (< 2.56%). The exact $\delta^{13}\text{C}$ and contribution of methane
340 from FTT synthesis are unknown.

341 The generation of gas through the secondary cracking of the crude oil expelled from
342 and retained in the source rock may also lead to the isotope reversal of natural gas
343 through its mix with gas generated directly from kerogen (Xia et al., 2013). The
344 relatively high BR_o of the bitumen from both the Red Cuvo Formation source rock (e.g.,
345 6015 m, BR_o of 2.62%) and the Chela Formation reservoir (BR_o of 1.88~1.98%; Table
346 1) could serve as the evidence for the thermal cracking of crude oils both retained in
347 the Red Cuvo Formation source rock and expelled into the reservoir, and thus the
348 generation of oil-cracking gases. The T_{max} of the Chela Formation bitumen is as high
349 as 470 °C (Liu et al., 2022). Besides, the fact that the Chela Formation reservoir bitumen
350 cannot fully dissolve in dichloromethane may also indicate the occurrence of thermal
351 cracking (Liu et al., 2022).

352 Furthermore, methane cracking and diffusion could also lead to the reversal of $\delta^{13}\text{C}$.
353 The cracking of methane under high temperatures can also lead to the reversal of $\delta^{13}\text{C}_1$
354 and $\delta^{13}\text{C}_2$ by generating ethane of light $\delta^{13}\text{C}$ and leaving the residual methane $\delta^{13}\text{C}$
355 progressively heavier (Cheng et al., 2020). However, such a situation is linked to shale
356 gas in overmature shales with $R_o > 2\%$ and thus unlikely to be a major reason for this
357 studied reservoir. Migration and diffusion can change the gas composition and isotope
358 composition and leave the residual methane with heavy $\delta^{13}\text{C}$ (Burruss and Laughrey,
359 2010; Stainforth, 2009). However, the Loeme salt Formation may have acted as a good
360 seal preventing significant diffusion of light hydrocarbons. Migration also shows no
361 significant influence on the $\delta^{13}\text{C}\text{-CH}_4$ and $\text{C}_1/(\text{C}_2 + \text{C}_3)$ in Figure 3d. Nevertheless, the
362 compositional and isotopic signatures of gaseous hydrocarbons may be fractionated
363 through the movement induced by CO_2 flux.

364 **5.4 Temporal evolution of the reservoir fluids**

365 Multiple possibilities have been proposed for the maturation timing of the Western
366 African pre-salt source rocks. In the central segment of the South Atlantic Ocean, they
367 could have reached the oil window during the Late Cretaceous in response to salt
368 remobilization and a possibly climate-driven increased sedimentation rate (Brownfield
369 and Charpentier, 2006; Marcano et al., 2013). For the Kwanza pre-salt source rocks in
370 specific, Danforth (1998) suggested that they entered the oil window only since the
371 Early Paleogene while White et al. (2003) proposed rapid oil generation after source
372 rock deposition due to abnormally high thermal regime. It was also suggested that early
373 oil generation could be possible for source rocks in the deeper parts of syn-rift grabens
374 due to the fast and thick salt deposition (Saller et al., 2016). Liu et al. (2022) constrained

375 the bitumen formation age in the studied reservoir to be 116 ± 29 Ma with the Re-Os
376 radioisotope system. Oil accumulation is earlier than bitumen formation, thus the oil
377 generation occurred rapidly after Red and Grey Cuvo formations source rock deposition
378 during the Barremian-Aptian. This is possibly a result of an abnormally high thermal
379 regime due to the continental crust thinning and active magmatism during the South
380 Atlantic Ocean opening and/or the fast and thick salt deposition (Liu et al., 2022; Saller
381 et al., 2016; White et al., 2003). Thus, all the key processes of this reservoir, i.e., the
382 source rock deposition and maturation, oil accumulation, magmatic CO₂ charge and
383 bitumen formation, occurred in a very short duration.

384 **5.5 Petroleum potential of the Kwanza Basin, Angola**

385 The South Atlantic Ocean opening process was associated with rifting and magma
386 activities accompanied by the release of massive CO₂ (Comin-Chiaramonti et al.,
387 2011). Reservoirs with CO₂ > 20% are relatively rare in petroleum basins, however,
388 they have been discovered in the pre-salt sections on both sides of the central segment
389 of the South Atlantic Ocean (Gamboa et al., 2019; Ma et al., 2015; Santos Neto et al.,
390 2012; this study). In the Brazilian Campos and Santos basins, pre-salt reservoirs with a
391 wide range of CO₂ percentages are discovered (Gamboa et al., 2019). There are two
392 types of sources recognized for the CO₂ in these reservoirs, one being almost
393 exclusively mantle-derived, and the other being mainly organic matter through
394 microbiological and diagenetic processes with occasional mantle influences (Gamboa
395 et al., 2019; Ma et al., 2015). In addition to the gas reservoir with ca. 80% CO₂ of this
396 study, ubiquitous CO₂ gas inclusions have been also discovered near the Benguela
397 Transfer Fault Zone in the southwestern part of the offshore Kwanza Basin, suggesting
398 that there were multiple episodes of CO₂ influx (Girard and Miguel, 2017). The offshore

399 Kwanza Basin pre-salt section demonstrates a similar origin and influence of CO₂ with
400 the Brazilian counterparts.

401 Gas reservoirs located in volcanic-sedimentary interacting domains characterized by a
402 mixture of geothermal (thermometamorphic or mantle-derived) CO₂ and biotic
403 (microbial or thermogenic) CH₄ are recognized as Sediment-Hosted Geothermal
404 Systems (SHGSs; Procesi et al., 2019). The maturity of source rocks in SHGSs is often
405 high due to active tectonic movement and anomalous heat flow (Procesi et al., 2019).
406 The injection of CO₂ into reservoirs could reduce the hydrocarbon potential by the
407 thermal alteration of crude oil into pyrobitumen and dry gas and the expulsion of crude
408 oil and gas from reservoirs (Liu et al., 2022 and this study). Nevertheless, the CO₂ could
409 also leach the carbonate reservoirs and may profoundly increase the porosity and
410 permeability, thus enhancing the reservoir quality. In addition to petroleum exploration,
411 the study of the fluid origin and evolution history of SHGSs could also contribute to
412 global climate change studies due to the possible emission of greenhouse gases CH₄
413 and CO₂ to the atmosphere (Procesi et al., 2019).

414 As demonstrated by the studied reservoir, the configuration of source rock, reservoir
415 and seal created during the rift and sag phases of the South Atlantic Ocean opening, and
416 the maturation of the source rock due to magmatism or sedimentation, imply potential
417 petroleum reserves for the pre-salt section of the offshore Kwanza basin. The Brazilian
418 Campos and Santos basins sharing common tectonic and sedimentary history with the
419 Kwanza Basin have reached tremendous success in petroleum exploration in the pre-
420 salt section (Aslanian et al., 2009; Ceraldi and Green, 2017; Karner and Gambôa, 2007;
421 Kukla et al., 2018; Quirk et al., 2013), which may imply great opportunities for the

422 Kwanza Basin. Dry wells and CO₂-rich reservoirs discovered during the primitive
423 exploration stage do not necessarily mean that the pre-salt plays of Angolan offshore
424 basins are poor in petroleum, as they are also discovered in the prolific Brazilian basins
425 (Gamboa et al., 2019; Ma et al., 2015; Santos Neto et al., 2012). There have already
426 been oil and gas accumulations discovered in the Kwanza Basin, too (Despinois et al.,
427 2014; Greenhalgh et al., 2012; Koning, 2014). Yet, the pre-salt reservoirs in the Kwanza
428 Basin are spatially limited and complex which is incomparable to the high-quality pre-
429 salt reservoirs of thick and homogenous microbial carbonates on the Brazilian side.
430 Considerable additional research is required to reveal the actual and full petroleum
431 potential of the extensive Kwanza Basin.

432 **6. Conclusions**

433 The pre-salt gas reservoir of the offshore Kwanza Basin, Angola is a Sediment-Host
434 Geothermal System (SHGS) containing mantle-derived CO₂ from an Aptian magmatic
435 episode and late mature thermogenic CH₄ from the Barremian-Aptian Red and Grey
436 Cuvo formations which reached maturation rapidly after deposition due to the
437 abnormally high thermal regime or the fast and thick salt deposition in the context of
438 South Atlantic Ocean opening. This reservoir demonstrates similar fluid origin and
439 possibly similar evolution history to the pre-salt SHGSs of the Brazilian Campos and
440 Santos basins. The conjugated Brazilian and Angolan basins also share common
441 tectonic and sedimentary history throughout the Cretaceous creating a similar
442 configuration of source, reservoir and seal. The great success of petroleum exploitation
443 in the pre-salt carbonate reservoir of the Brazilian basins may thus imply great reserves
444 in the counterparts of the offshore Kwanza Basin, Angola. Nevertheless, the Kwanza

445 Basin has its unique characteristics and further research is required to reveal its full
446 petroleum potential.

447 **Data availability statement**

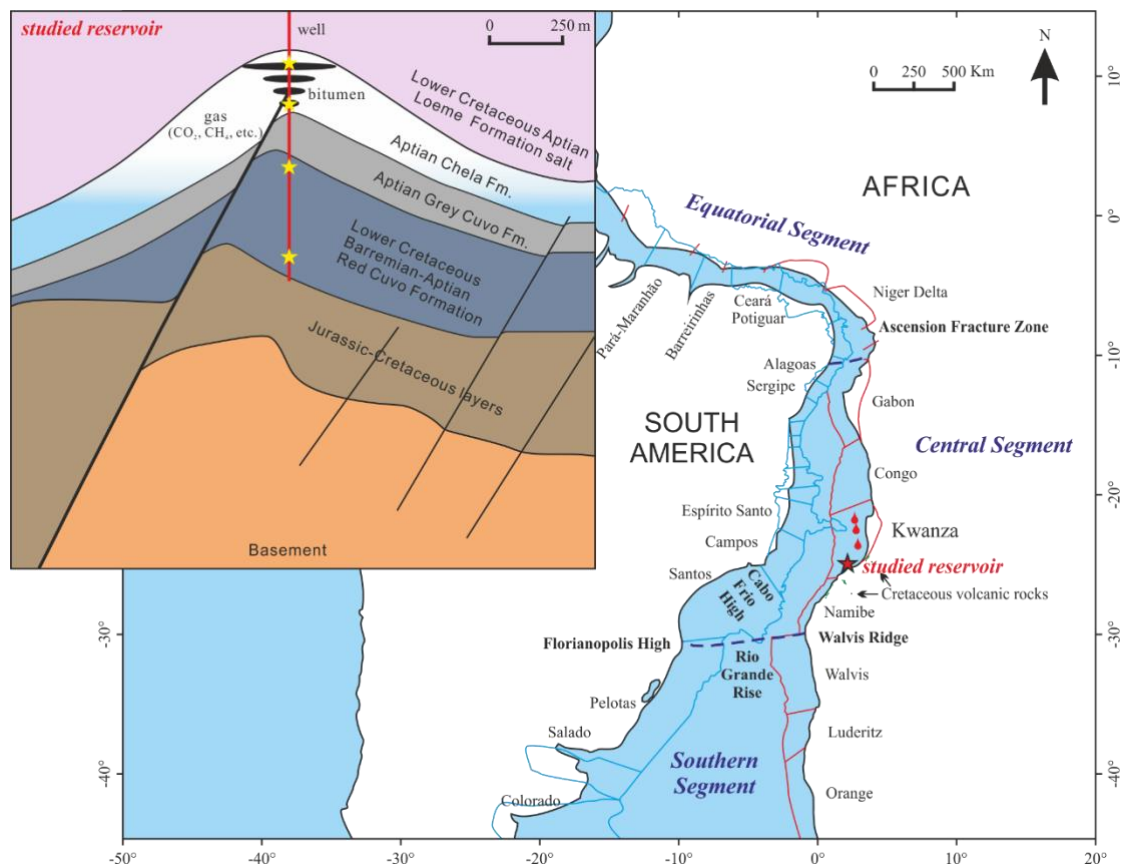
448 The data presented in this study are available upon request from the corresponding
449 author.

450 **Funding**

451 This work was supported by the National Key Research and Development Project of
452 China [2020YFA0714804]; National Natural Science Foundation of China [42003043];
453 Total Postdoctoral research award; China Postdoctoral Science Foundation
454 [2020M672850]; and Guangdong Basic and Applied Basic Research Foundation
455 (Guangdong-Guangzhou Joint Fund) [2019A1515110310] to Junjie Liu; and the Total
456 Endowment Fund and CUG Wuhan Dida Scholarship to David Selby. The project was
457 also supported by the NERC Innovation award [NE/L008343/1] as part of the Oil and
458 Gas Catalyst award scheme.

459 **Acknowledgements**

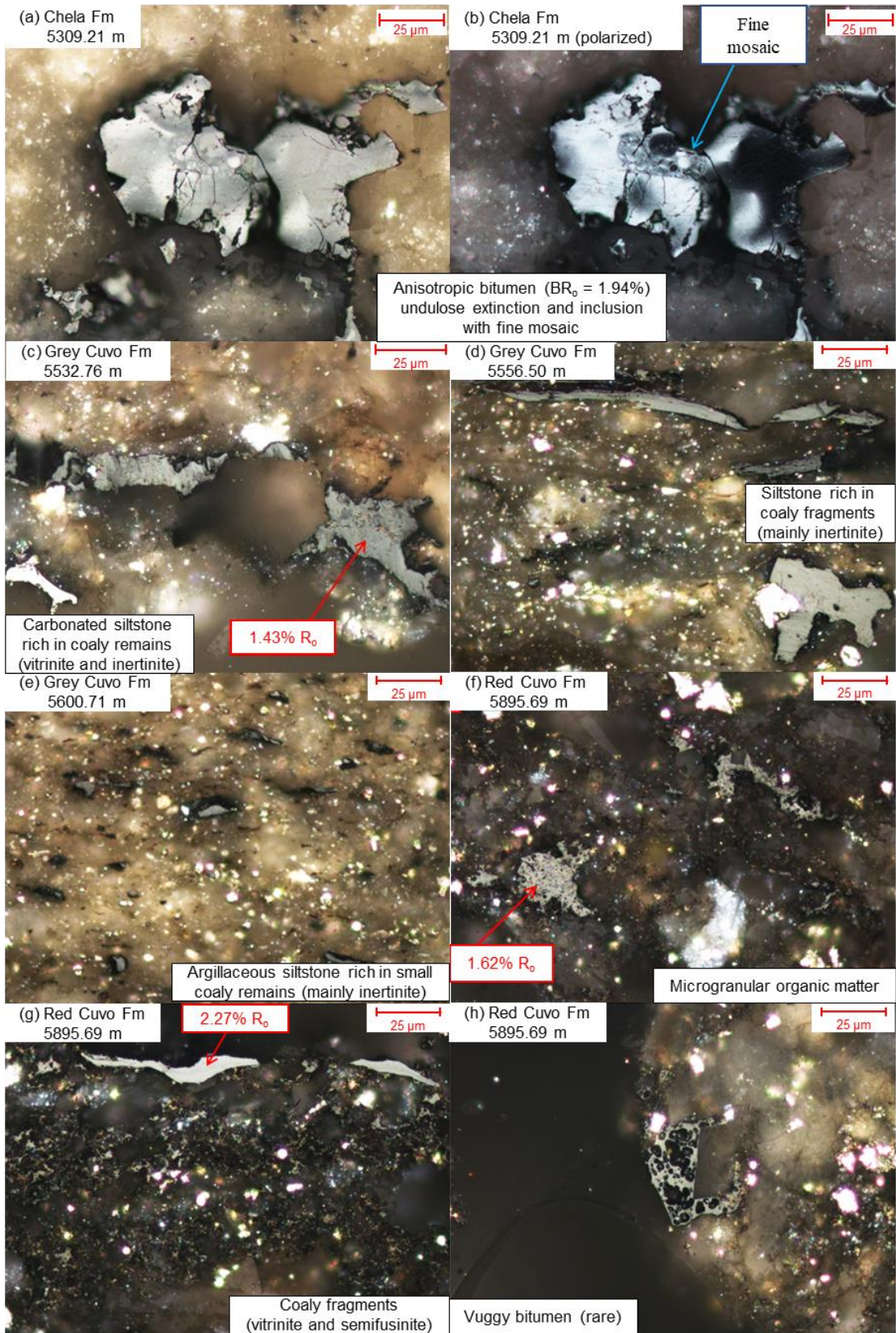
460 We thank Prof. Jeffrey D. Stilwell, Dr. Daniel Thompson, and Dr. Stephen Poropat for
461 providing help on the geological background and Figure 1, and Prof. Tian Hui and Prof.
462 Hu Guang for their constructive advices. We also thank the Editor, Dr. Giuseppe Etiope,
463 and Dr. Martin Blumenberg and another anonymous reviewer for the timely, detailed
464 and very constructive comments.



466

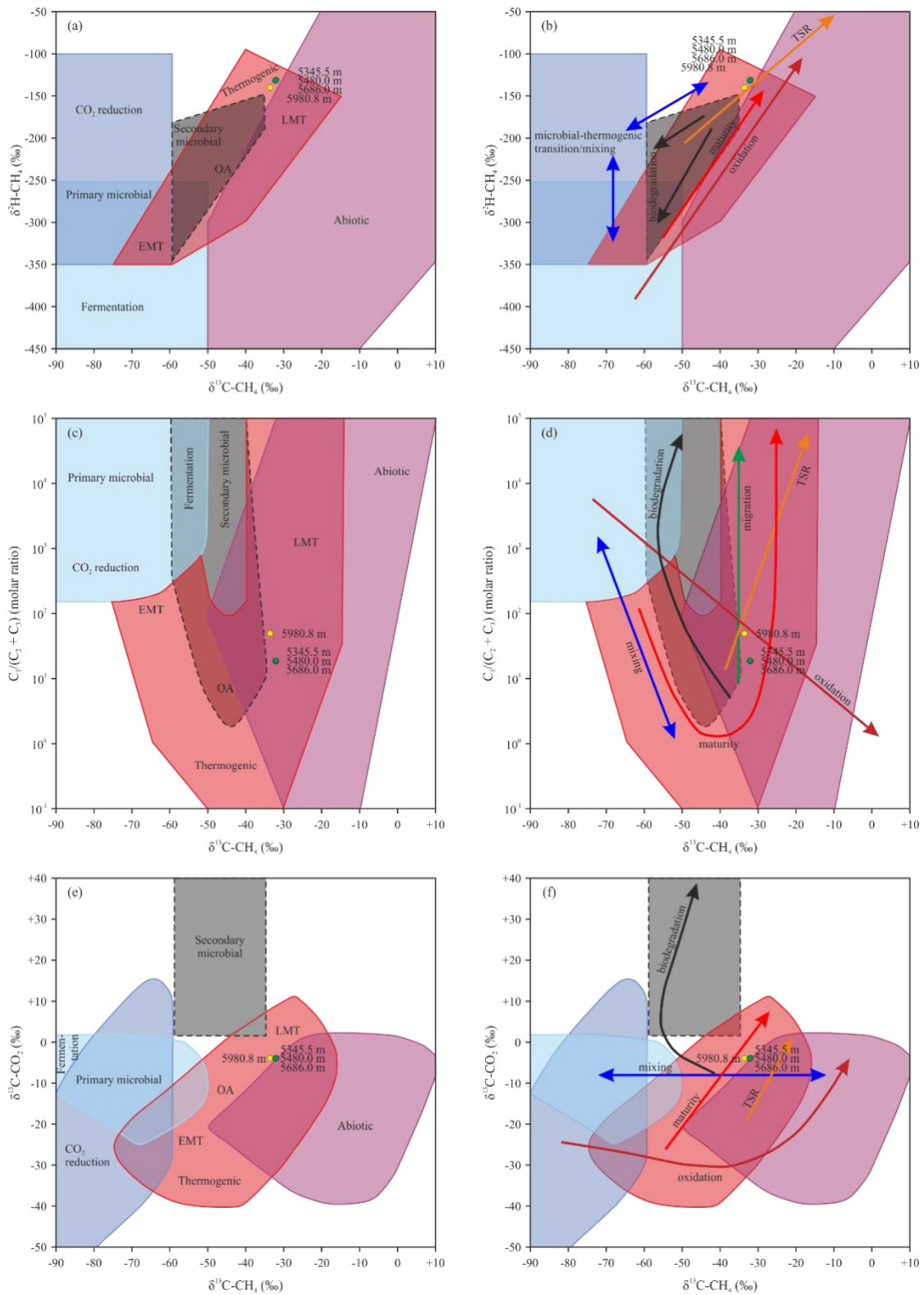
467 Figure 1 The Aptian South Atlantic Ocean margin (Masse and Laurent, 2016;
 468 Thompson et al., 2015) and the seismic profile interpretation of structure and
 469 stratigraphy of the studied reservoir (the inset; Liu et al., 2022). The red star marks the
 470 location of the studied reservoir. The red drops are locations with pre-salt petroleum
 471 discoveries. The yellow stars of the inset are the fluid sampling positions.

472 It is a 2-column fitting image.



474 Figure 2 Matrices and macerals of the Chela, Grey and Red Cuvo formations. The only
475 organic matter observed in the Chela Formation is the anisotropic bitumen with
476 undulose extinction and no fluorescence filling the intercrystalline pores of carbonate
477 (a-b). The Grey Cuvo Formation carbonated and argillaceous siltstones are rich in
478 humic coaly remains (c- e). The occasionally carbonated siliciclastic rocks of the Red
479 Cuvo Formation contain sapropelic micro-granular organic matter as thin reflective
480 networks (f), humic coaly remains in lower content than the Grey Cuvo Formation (g),
481 and scarce vuggy bitumen (h). Fluorescence of organic matter is absent under high
482 maturity.

483 It is a 2-column fitting image.



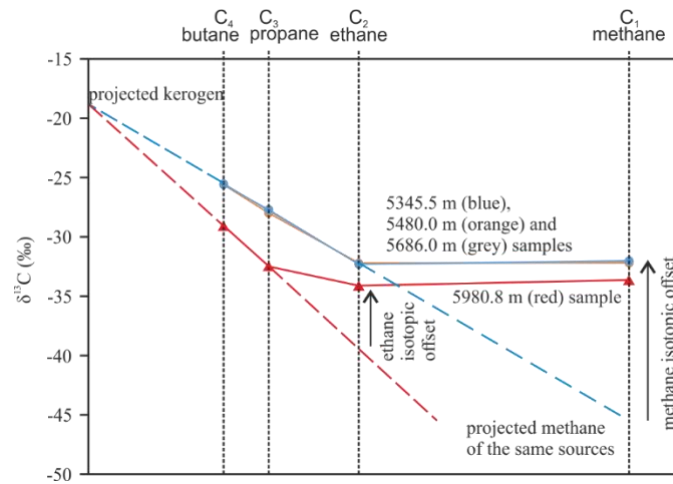
484

485 Figure 3 The genetic diagrams indicating the origin and alteration processes of the gas
 486 samples (Milkov and Etiope, 2018). EMT – early mature thermogenic gas; OA – oil-
 487 associated thermogenic gas; LMT – late mature thermogenic gas; TSR –

488 thermochemical sulfate reduction. The gas samples in this study are late mature

489 thermogenic gas in general.

490 It is a 2-column fitting image.



491

492 Figure 4 Gas samples on the diagram of $1/C_n$ versus $\delta^{13}\text{C}$ (Chung et al., 1988). The
 493 shallower three samples are very similar above (the overlapped orange, grey and blue
 494 lines and marks) while the deepest sample fits on a lower red line. The $\delta^{13}\text{C}$ of the
 495 methane (and ethane for the deepest sample) is higher than the projection. The $\delta^{13}\text{C}$ of
 496 the methane and ethane are slightly reversed, mainly indicating the mixing of humic
 497 and sapropelic sources for the gas.

498 It is a 1-column fitting image.

499 **Tables**

500 Table 1 The TOC contents and maturity (VR_o/BR_o) of the sidewall core samples.

Formation	Depth (m)	TOC (wt.%)	Maceral	VR _o /BR _o ^a (%)	Equivalent VR _o ^b (%)
Chela ^c	5304.00	4.50	bitumen	/	/
	5309.21	3.99	bitumen	1.94	1.60
	5371.75	1.32	bitumen	1.96	1.61
	5408.69	0.99	bitumen	1.88	1.56
	5493.69	0.38	bitumen	1.98	1.62
Grey Cuvo	5532.76	0.60	vitroinite	1.45	/
	5556.50	0.65	vitroinite	1.46	/
	5600.71	0.97	vitroinite	1.52	/
Red Cuvo	5791.50	1.21	vitroinite	1.73	/
	5807.70	3.86	vitroinite	1.69	/
	5844.60	1.21	vitroinite	1.86	/
	5895.69	1.44	vitroinite	2.14	/
	5901.03	1.29	vitroinite	1.97	/
	5958.01	1.99	vitroinite	2.02	/
	5991.61	1.11	vitroinite	2.07	/
	6015.00	1.59	vitroinite bitumen	2.13 2.62	/ 2.02

501

502 ^a VR_o/BR_o: Vitroinite/Bitumen reflectance under white incident light in oil immersion ;

503 ^b Jacob's formula (Jacob, 1989): VR_o = 0.618 × BR_o + 0.4;

504 ^c Part of the Chela Formation samples data is from Liu et al. (2022).

505

Table 2 The Rock-Eval parameters of the Red Cuvo Formation.

Depth (m)	S1 (mg HC/g rock)	S2 (mg HC/g rock)	PI ^a	HI ^b (mg HC/g TOC)
5791.50	2.8	0.92	0.75	76
5807.70	5.55	0.98	0.85	25
5844.60	1.81	0.37	0.83	31
5895.69	2.05	0.25	0.89	17
5901.30	1.33	0.27	0.83	21
5958.01	0.84	0.39	0.68	20
5991.61	0.34	0.28	0.55	25
6015.00	0.32	0.19	0.63	12
<i>Average</i>	<i>1.88</i>	<i>0.46</i>	<i>0.75</i>	<i>28</i>

506

507 ^a PI: S1/(S1 + S2);508 ^b HI: S2×100/TOC.

Table 3 Chemical and isotopic composition of the gas samples.

Formation		Chela		Red Cuvo	
Depth (m)		5345.5	5480.0	5686.0	5980.8
Composition of the fluids (In molar fractions (%) and molar ratios)	CO ₂	82.85	84.07	82.65	82.15
	H ₂ S	0.00	0.00	0.00	0.00
	CH ₄	15.78	14.23	15.99	16.57
	C ₂ H ₆	0.66	0.60	0.66	0.30
	C ₃ H ₈	0.19	0.16	0.18	0.03
	<i>i</i> -C ₄ H ₁₀	0.03	0.02	0.03	0.00
	<i>n</i> -C ₄ H ₁₀	0.05	0.02	0.05	0.00
	<i>i</i> -C ₅ H ₁₂	0.02	0.01	0.02	0.00
	<i>n</i> -C ₅ H ₁₂	0.01	0.01	0.01	0.00
	CO ₂ /CH ₄	5.25	5.91	5.17	4.96
	C ₁ /(C ₂ + C ₃)	18.66	18.73	19.01	49.42
	C ₂ /C ₃	3.47	3.74	3.68	9.17
	ln(C ₁ /C ₂)	3.18	3.17	3.19	4.00
	ln(C ₂ /C ₃)	1.24	1.32	1.30	2.22
Wetness (%) ^a	5.75	5.40	5.63	2.04	
$\delta^{13}\text{C}$ (‰)	CH ₄	-32.00	-32.20	-32.10	-33.60
	C ₂ H ₆	-32.30	-32.20	-32.30	-34.20
	C ₃ H ₈	-27.70	-28.00	-27.80	-32.40
	<i>n</i> -C ₄ H ₁₀	-25.60	-25.60	-25.50	-29.00
	<i>n</i> -C ₅ H ₁₂ ^b	-24.90	<	-24.90	<
	CO ₂	-3.90	-4.00	-3.90	-3.90
	$\delta^{13}\text{C}_1 - \delta^{13}\text{C}_2$	0.30	0.00	0.20	0.60
$\delta^{13}\text{C}_2 - \delta^{13}\text{C}_3$	-4.60	-4.20	-4.50	-1.80	
$\delta^2\text{H}$ (‰)	CH ₄	-131.00	-132.00	-131.00	-140.00
	C ₂ H ₆	-129.00	-136.00	-133.00	-118.00
Helium	⁴ He (cm ³ STP/cm ³) ^c	0.99×10^{-4}	1.07×10^{-4}	1.13×10^{-4}	1.44×10^{-4}
	³ He/ ⁴ He (R/R _a) ^d	4.60	4.39	4.36	4.65
	CO ₂ / ³ He (mol/mol)	1.32×10^9	1.30×10^9	1.22×10^9	0.89×10^9
	CH ₄ / ³ He (mol/mol)	2.5×10^8	2.2×10^8	2.3×10^8	1.8×10^8

511

512 ^a Wetness: $\sum(C_2 - C_5)/\sum(C_1 - C_5)$, %;513 ^b Italics: close to detection limits but repeatable; <: under detection limits;514 ^c cm³(STP)/cm³ = cubic centimeter under standard temperature and pressure (1atm and

515 15°C) per cubic centimeter;

516 ^d R/R_a = ³He/⁴He of the sample divided by ³He/⁴He ratio of the air (1.384×10^{-6}).

517 **References**

- 518 Aslanian, D., Moulin, M., Olivet, J.-L., Unternehr, P., Matias, L., Bache, F., Rabineau,
519 M., Nouzé, H., Klingelhoefer, F., Contrucci, I., Labails, C., 2009. Brazilian and
520 African passive margins of the Central Segment of the South Atlantic Ocean:
521 Kinematic constraints. *Tectonophysics* 468, 98-112.
522 <https://doi.org/10.1016/j.tecto.2008.12.016>
- 523 ASTM, 2011a. D2797/D2797M-11a Standard practice for preparing coal samples for
524 microscopical analysis by reflected light, West Conshohocken, PA.
- 525 ASTM, 2011b. D7708-11 Standard Test Method for Microscopical Determination of
526 the Reflectance of Vitrinite Dispersed in Sedimentary Rocks, West
527 Conshohocken, PA.
- 528 ASTM, 2012. D2799-12 Standard Test Method for Microscopical Determination of the
529 Maceral Composition of Coal, West Conshohocken, PA.
- 530 Ballentine, C.J., Burgess, R., Marty, B., 2002. Tracing Fluid Origin, Transport and
531 Interaction in the Crust. *Reviews in Mineralogy and Geochemistry*, 47(1): 539-
532 614. <https://doi.org/10.2138/rmg.2002.47.13>
- 533 Behar, F., Kressmann, S., Rudkiewicz, J.L., Vandenbroucke, M., 1992. Experimental
534 simulation in a confined system and kinetic modelling of kerogen and oil
535 cracking. *Organic Geochemistry*, 19(1): 173-189. [https://doi.org/10.1016/0146-
536 6380\(92\)90035-V](https://doi.org/10.1016/0146-6380(92)90035-V)
- 537 Bernard, B.B., Brooks, J.M., Sackett, W.M., 1976. Natural gas seepage in the Gulf of
538 Mexico. *Earth and Planetary Science Letters* 31, 48-54.
539 [https://doi.org/10.1016/0012-821X\(76\)90095-9](https://doi.org/10.1016/0012-821X(76)90095-9)
- 540 Blaich, O.A., Faleide, J.I., Tsikalas, F., 2011. Crustal breakup and continent - ocean
541 transition at South Atlantic conjugate margins. *Journal of Geophysical Research:*
542 *Solid Earth*, 116(B01402). <https://doi.org/10.1029/2010JB007686>
- 543 Brownfield, M.E., Charpentier, R.R., 2006. Geology and total petroleum systems of the
544 West-Central Coastal province (7203), West Africa. 2207B.
545 <https://doi.org/10.3133/b2207B>
- 546 Burruss, R.C., Laughrey, C.D., 2010. Carbon and hydrogen isotopic reversals in deep
547 basin gas: Evidence for limits to the stability of hydrocarbons. *Organic*
548 *Geochemistry*, 41(12): 1285-1296.
549 <https://doi.org/10.1016/j.orggeochem.2010.09.008>
- 550 Burwood, R., 1999. Angola: source rock control for Lower Congo Coastal and Kwanza
551 Basin petroleum systems. Geological Society, London, Special Publications,
552 153(1): 181-194. <https://doi.org/10.1144/gsl.sp.1999.153.01.12>
- 553 Ceraldi, T.S., Green, D., 2017. Evolution of the South Atlantic lacustrine deposits in
554 response to Early Cretaceous rifting, subsidence and lake hydrology. *Geological*

- 555 Society, London, Special Publications, 438(1): 77-98.
556 <https://doi.org/10.1144/SP438.10>
- 557 Cheng, B., Xu, J., Deng, Q., Liao, Z., Wang, Y., Faboya, O.L., Li, S., Liu, J., Peng, P.a.,
558 2020. Methane cracking within shale rocks: A new explanation for carbon
559 isotope reversal of shale gas. *Marine and Petroleum Geology*, 121: 104591.
560 <https://doi.org/10.1016/j.marpetgeo.2020.104591>
- 561 Chung, H.M., Gormly, J.R., Squires, R.M., 1988. Origin of gaseous hydrocarbons in
562 subsurface environments: Theoretical considerations of carbon isotope
563 distribution. *Chemical Geology*, 71(1): 97-104. [https://doi.org/10.1016/0009-2541\(88\)90108-8](https://doi.org/10.1016/0009-2541(88)90108-8)
564
- 565 Clarke, W.B., Jenkins, W.J., Top, Z., 1976. Determination of tritium by mass
566 spectrometric measurement of ^3He . *The International Journal of Applied
567 Radiation and Isotopes* 27, 515–522. doi:10.1016/0020-708X(76)90082-X.
- 568 Clayton, C., 1991. Carbon isotope fractionation during natural gas generation from
569 kerogen. *Marine and Petroleum Geology*, 8(2): 232-240.
570 [https://doi.org/10.1016/0264-8172\(91\)90010-X](https://doi.org/10.1016/0264-8172(91)90010-X)
- 571 Comin-Chiaramonti, P., De Min, A., Girardi, V.A.V., Ruberti, E., 2011. Post-Paleozoic
572 magmatism in Angola and Namibia: A review, *Volcanism and Evolution of the
573 African Lithosphere*. Geological Society of America Special Papers, pp. 223-
574 247. [https://doi.org/10.1130/2011.2478\(12\)](https://doi.org/10.1130/2011.2478(12))
- 575 Dai, J., Li, J., Luo, X., Zhang, W., Hu, G., Ma, C., Guo, J., Ge, S., 2005. Stable carbon
576 isotope compositions and source rock geochemistry of the giant gas
577 accumulations in the Ordos Basin, China. *Organic Geochemistry*, 36(12): 1617-
578 1635. <https://doi.org/10.1016/j.orggeochem.2005.08.017>
- 579 Dai, J., Ni, Y., Huang, S., Gong, D., Liu, D., Feng, Z., Peng, W., Han, W., 2016.
580 Secondary origin of negative carbon isotopic series in natural gas. *Journal of
581 Natural Gas Geoscience*, 1(1): 1-7. <https://doi.org/10.1016/j.jnggs.2016.02.002>
- 582 Dai, J., Xia, X., Qin, S., Zhao, J., 2004. Origins of partially reversed alkane $\delta^{13}\text{C}$ values
583 for biogenic gases in China. *Organic Geochemistry*, 35(4): 405-411.
584 <https://doi.org/10.1016/j.orggeochem.2004.01.006>
- 585 Dai, J., Zou, C., Zhang, S., Li, J., Ni, Y., Hu, G., Luo, X., Tao, S., Zhu, G., Mi, J., Li,
586 Z., Hu, A., Yang, C., Zhou, Q., Shuai, Y., Zhang, Y., Ma, C., 2008.
587 Discrimination of abiogenic and biogenic alkane gases. *Science in China Series
588 D: Earth Sciences*, 51(12): 1737-1749. <https://doi.org/10.1007/s11430-008-0133-1>
589
- 590 Danforth, A., 1998. Petroleum systems of the coastal Kwanza and Benguela basins,
591 Angola, *Houston Geological Society Bulletin*, pp. 18,19, 21,
592 <https://archives.datapages.com/data/HGS/vol41/no02/images/vol41no2p18.pdf>

- 593 Denis, M., Kluska, J.-M., 2017. South Kwanza Basin (Offshore Angola) as a Major
594 Cornerstone of West African Margin, AAPG Annual Convention and
595 Exhibition, Houston, Texas, USA.
- 596 Despinois, F., Rimmelé, G., Santos, Y., Nielsen, C., Maurel, L., Rubio, E., Ducastaing,
597 M., 2014. Exploration Challenges of Angolan Pre-salt & Contributions from
598 Brazilian Experience, Rio Oil & Gas Expo and Conference, Rio de Janeiro,
599 Brazil.
- 600 Etiope, G., Oze, C., 2022. Microbial vs abiotic origin of methane in continental
601 serpentized ultramafic rocks: A critical review and the need of a holistic
602 approach. *Applied Geochemistry* 143, 105373.
603 <https://doi.org/10.1016/j.apgeochem.2022.105373>
- 604 Etiope, G., Sherwood Lollar, B., 2013. Abiotic methane on earth. *Reviews of
605 Geophysics*, 51(2): 276-299. <https://doi.org/10.1002/rog.20011>
- 606 Etiope, G., Whiticar, M.J., 2019. Abiotic methane in continental ultramafic rock
607 systems: Towards a genetic model. *Applied Geochemistry* 102, 139-152.
608 <https://doi.org/10.1016/j.apgeochem.2019.01.012>
- 609 Ferraz, A., Gamboa, L., Neto, E.V.d.S., Baptista, R., 2019. Crustal structure and CO₂
610 occurrences in the Brazilian basins. *Interpretation*, 7(4): SL37-SL45.
611 <https://doi.org/10.1190/int-2019-0038.1>
- 612 Gamboa, L., Ferraz, A., Baptista, R., Neto, E.V.S., 2019. Geotectonic Controls on CO₂
613 Formation and Distribution Processes in the Brazilian Pre-Salt Basins.
614 *Geosciences*, 9(6): 252. <https://doi.org/10.3390/GEOSCIENCES9060252>
- 615 Girard, J.-P., Miguel, G., 2017. Evidence of high temperature hydrothermal regimes in
616 the Presalt series, Kwanza basin, Offshore Angola, AAPG Annual Convention
617 and Exhibition, Houston, Texas.
- 618 Graham, D.W., 2002. Noble Gas Isotope Geochemistry of Mid-Ocean Ridge and Ocean
619 Island Basalts: Characterization of Mantle Source Reservoirs. *Reviews in
620 Mineralogy and Geochemistry*, 47(1): 247-317.
621 <https://doi.org/10.2138/rmg.2002.47.8>
- 622 Greenhalgh, J., Borsato, R., Mathew, F., Duncan-Jones, G., Pimenta, I., da Silva, J.M.,
623 da Silva, L.N., 2012. Petroleum plays and prospectivity in the Kwanza and
624 Benguela Basins offshore Angola, AAPG International Conference &
625 Exhibition, Singapore, p. 7.
- 626 Györe, D., 2015. Noble gases as tracers of injected CO₂ in the Cranfield enhanced oil
627 recovery field, University of Glasgow, <https://theses.gla.ac.uk/7127/>
- 628 Hunt, J.M., 1996. *Petroleum Geochemistry and Geology*. W.H Freeman and Co, New
629 York, p. 743.
- 630 Jacob, H., 1989. Classification, structure, genesis and practical importance of natural
631 solid oil bitumen (“migrabitumen”). *International Journal of Coal Geology*,
632 11(1): 65-79. [https://doi.org/10.1016/0166-5162\(89\)90113-4](https://doi.org/10.1016/0166-5162(89)90113-4)

- 633 Jenden, P.D., Drazan, D.J., Kaplan, I.R., 1993a. Mixing of Thermogenic Natural Gases
634 in Northern Appalachian Basin. *AAPG Bulletin*, 77(6): 980-998.
635 <https://doi.org/10.1306/bdff8dbc-1718-11d7-8645000102c1865d>
- 636 Jenden, P.D., Hilton, D.R., Kaplan, I.R., Craig, H., 1993b. Abiogenic hydrocarbons and
637 mantle helium in oil and gas fields. In: Howell, D.G. (Ed.), *US Geological*
638 *survey professional paper*, Washington, pp. 31-56,
639 <https://www.osti.gov/biblio/7052010>
- 640 Jerram, D.A., Sharp, I.R., Torsvik, T.H., Poulsen, R., Watton, T., Freitag, U., Halton,
641 A., Sherlock, S.C., Malley, J.A.S., Finley, A., Roberge, J., Swart, R.,
642 Puigdefabregas, C., Ferreira, C.H., Machado, V., 2019. Volcanic constraints on
643 the unzipping of Africa from South America: Insights from new
644 geochronological controls along the Angola margin. *Tectonophysics*, 760: 252-
645 266. <https://doi.org/10.1016/j.tecto.2018.07.027>
- 646 Karner, G.D., Gambôa, L.A.P., 2007. Timing and origin of the South Atlantic pre-salt
647 sag basins and their capping evaporites. *Geological Society, London, Special*
648 *Publications*, 285(1): 15-35. <https://doi.org/10.1144/sp285.2>
- 649 Koning, T., 2014. Angola's oil industry - a century of progress in exploration and
650 production, AAPG International Conference & Exhibition, Istanbul, Turkey.
- 651 Kukla, P.A., Strozyk, F., Mohriak, W.U., 2018. South Atlantic salt basins – Witnesses
652 of complex passive margin evolution. *Gondwana Research*, 53: 41-57.
653 <https://doi.org/10.1016/j.gr.2017.03.012>
- 654 Liu, J., Zhou, H., Pujol, M., Selby, D., Li, J., Tian, H., 2022. The bitumen formation
655 and Re-Os characteristics of a CO₂-rich pre-salt gas reservoir of the Kwanza
656 Basin, offshore Angola. *Marine and Petroleum Geology*, 143: 105786.
657 <https://doi.org/10.1016/j.marpetgeo.2022.105786>
- 658 Liu, Q., Wu, X., Wang, X., Jin, Z., Zhu, D., Meng, Q., Huang, S., Liu, J., Fu, Q., 2019.
659 Carbon and hydrogen isotopes of methane, ethane, and propane: A review of
660 genetic identification of natural gas. *Earth-Science Reviews*, 190: 247-272.
661 <https://doi.org/10.1016/j.earscirev.2018.11.017>
- 662 Lorant, F., Prinzhofer, A., Behar, F., Huc, A.-Y., 1998. Carbon isotopic and molecular
663 constraints on the formation and the expulsion of thermogenic hydrocarbon
664 gases. *Chemical Geology*, 147(3): 249-264. [https://doi.org/10.1016/S0009-2541\(98\)00017-5](https://doi.org/10.1016/S0009-2541(98)00017-5)
- 666 Ma, A., Li, Y., Zhang, X., Zhang, Z., 2015. Carbon dioxide origin, alkane gas
667 geochemical characteristics and pool-forming model of pre-salt J oilfield in
668 offshore Santos basin, Brazil. *China Offshore Oil and Gas*, 27: 13-20.
669 <https://doi.org/10.11935/j.issn.1673-1506.2015.05.002>
- 670 Marcano, G., Anka, Z., di Primio, R., 2013. Major controlling factors on hydrocarbon
671 generation and leakage in South Atlantic conjugate margins: A comparative

- 672 study of Colorado, Orange, Campos and Lower Congo basins. *Tectonophysics*,
673 604: 172-190. <https://doi.org/10.1016/j.tecto.2013.02.004>
- 674 Marsh, J.S., Swart, R., 2018. The Bero Volcanic Complex: Extension of the Paran -
675 Etendeka Igneous Province into SW Angola. *Journal of Volcanology and*
676 *Geothermal Research*, 355: 21-31.
677 <https://doi.org/10.1016/j.jvolgeores.2016.10.011>
- 678 Marzoli, A., Melluso, L., Morra, V., Renne, P.R., Sgrosso, I., D'Antonio, M., Duarte
679 Morais, L., Morais, E.A.A., Ricci, G., 1999. Geochronology and petrology of
680 Cretaceous basaltic magmatism in the Kwanza basin (western Angola), and
681 relationships with the Paran -Etendeka continental flood basalt province.
682 *Journal of Geodynamics*, 28(4): 341-356. [https://doi.org/10.1016/S0264-](https://doi.org/10.1016/S0264-3707(99)00014-9)
683 [3707\(99\)00014-9](https://doi.org/10.1016/S0264-3707(99)00014-9)
- 684 Masse, P., Laurent, O., 2016. Geological exploration of Angola from Sumbe to Namibe:
685 A review at the frontier between geology, natural resources and the history of
686 geology. *Comptes Rendus Geoscience*, 348(1): 80-88.
687 <https://doi.org/10.1016/j.crte.2015.09.007>
- 688 Milkov, A.V., Etiope, G., 2018. Revised genetic diagrams for natural gases based on a
689 global dataset of >20,000 samples. *Organic Geochemistry* 125, 109-120.
690 <https://doi.org/10.1016/j.orggeochem.2018.09.002>
- 691 Porcelli, D., Ballentine, C.J., Wieler, R., 2002. An Overview of Noble Gas
692 Geochemistry and Cosmochemistry. *Reviews in Mineralogy and Geochemistry*,
693 47(1): 1-19. <https://doi.org/10.2138/rmg.2002.47.1>
- 694 Procesi, M., Ciotoli, G., Mazzini, A., Etiope, G., 2019. Sediment-hosted geothermal
695 systems: Review and first global mapping. *Earth-Science Reviews* 192, 529-
696 544. <https://doi.org/10.1016/j.earscirev.2019.03.020>
- 697 Quirk, D.G., Hertle, M., Jeppesen, J.W., Raven, M., Mohriak, W.U., Kann, D.J.,
698 N rgaard, M., Howe, M.J., Hsu, D., Coffey, B., Mendes, M.P., 2013. Rifting,
699 subsidence and continental break-up above a mantle plume in the central South
700 Atlantic. *Geological Society, London, Special Publications*, 369(1): 185-214.
701 <https://doi.org/10.1144/sp369.20>
- 702 Reusch, A.M., Nyblade, A.A., Wiens, D.A., Shore, P.J., Ateba, B., Tabod, C.T.,
703 Nnange, J.M., 2010. Upper mantle structure beneath Cameroon from body wave
704 tomography and the origin of the Cameroon Volcanic Line. *Geochemistry,*
705 *Geophysics, Geosystems*, 11(10). <https://doi.org/10.1029/2010GC003200>
- 706 Saller, A., Rushton, S., Buambua, L., Inman, K., McNeil, R., Dickson, J.A.D., 2016.
707 Presalt stratigraphy and depositional systems in the Kwanza Basin, offshore
708 Angola. *AAPG Bulletin*, 100(07): 1135-1164.
709 <https://doi.org/10.1306/02111615216>
- 710 Santos Neto, E. V., Cerqueira, J. R., Prinzhofer, A., 2012. Origin of CO₂ in Brazilian
711 basins: AAPG Annual Convention and Exhibition, Article #40969

- 712 Sherwood Lollar, B., Ballentine, C.J., Onions, R.K., 1997. The fate of mantle-derived
713 carbon in a continental sedimentary basin: Integration of C/He relationships and
714 stable isotope signatures. *Geochimica et Cosmochimica Acta*, 61(11): 2295-
715 2307. [https://doi.org/10.1016/S0016-7037\(97\)00083-5](https://doi.org/10.1016/S0016-7037(97)00083-5)
- 716 Stainforth, J.G., 2009. Practical kinetic modeling of petroleum generation and
717 expulsion. *Marine and Petroleum Geology*, 26(4): 552-572.
718 <https://doi.org/10.1016/j.marpetgeo.2009.01.006>
- 719 Tang, Y., Perry, J.K., Jenden, P.D., Schoell, M., 2000. Mathematical modeling of stable
720 carbon isotope ratios in natural gases. *Geochimica et Cosmochimica Acta*,
721 64(15): 2673-2687. [https://doi.org/10.1016/S0016-7037\(00\)00377-X](https://doi.org/10.1016/S0016-7037(00)00377-X)
- 722 Thompson, D.L., Stilwell, J.D., Hall, M., 2015. Lacustrine carbonate reservoirs from
723 Early Cretaceous rift lakes of Western Gondwana: Pre-Salt coquinas of Brazil
724 and West Africa. *Gondwana Research*, 28(1): 26-51.
725 <https://doi.org/10.1016/j.gr.2014.12.005>
- 726 Tilley, B., McLellan, S., Hiebert, S., Quatero, B., Veilleux, B., Muehlenbachs, K.,
727 2011. Gas isotope reversals in fractured gas reservoirs of the western Canadian
728 Foothills: Mature shale gases in disguise. *AAPG Bulletin*, 95(8): 1399-1422.
729 <https://doi.org/10.1306/01031110103>
- 730 Tilley, B., Muehlenbachs, K., 2013. Isotope reversals and universal stages and trends
731 of gas maturation in sealed, self-contained petroleum systems. *Chemical
732 Geology*, 339: 194-204. <https://doi.org/10.1016/j.chemgeo.2012.08.002>
- 733 Torsvik, T.H., Rouse, S., Labails, C., Smethurst, M.A., 2009. A new scheme for the
734 opening of the South Atlantic Ocean and the dissection of an Aptian salt basin.
735 *Geophysical Journal International*, 177(3): 1315-1333.
736 <https://doi.org/10.1111/j.1365-246X.2009.04137.x>
- 737 White, N., Thompson, M., Barwise, T., 2003. Understanding the thermal evolution of
738 deep-water continental margins. *Nature*, 426(6964): 334-343.
739 <https://doi.org/10.1038/nature02133>
- 740 Wycherley, H., Fleet, A., Shaw, H., 1999. Some observations on the origins of large
741 volumes of carbon dioxide accumulations in sedimentary basins. *Marine and
742 Petroleum Geology*, 16(6): 489-494. [https://doi.org/10.1016/S0264-
743 8172\(99\)00047-1](https://doi.org/10.1016/S0264-8172(99)00047-1)
- 744 Xia, X., Chen, J., Braun, R., Tang, Y., 2013. Isotopic reversals with respect to maturity
745 trends due to mixing of primary and secondary products in source rocks.
746 *Chemical Geology*, 339: 205-212.
747 <https://doi.org/10.1016/j.chemgeo.2012.07.025>
- 748 Xia, X., Zhao, L., Zhang, W., Li, J., 1999. Geochemical characteristics and source rock
749 of Ordovician gas reservoir, Changqing Gasfield. *Chinese Science Bulletin*,
750 44(20): 1917-1920. <https://doi.org/10.1007/BF02886354>

751 Zumberge, J., Ferworn, K., Brown, S., 2012. Isotopic reversal ('rollover') in shale gases
752 produced from the Mississippian Barnett and Fayetteville formations. *Marine*
753 *and Petroleum Geology*, 31(1): 43-52.
754 <https://doi.org/10.1016/j.marpetgeo.2011.06.009>